Theor Chem Acc (2006) 115: 410–426
DOI 10.1007/s00214-006-0122-4

REGULAR ARTICLE

Yang Liu · Xu-Ri Huang · Guang-Tao Yu
Hui-Ling Liu · Chia-Chung Sun

Structure and stability of isomers of the promising interstellar molecule PC_3O

Received: 4 October 2005 / Accepted: 13 January 2006 / Published online: 1 March 2006

Abstract DFT/B3LYP/6-311G(d) and CCSD(T)/6-311G(2d) single-point calculations are carried out for exploring the doublet potential energy surface (PES) of PC_3O, a molecule of potential interest in interstellar chemistry. A total of 29 minima connected by 65 interconversion transition states are located. The structures of the most relevant isomers and transition states are further optimized at the QCISD level followed by CCSD(T) single-point energy calculations. At the CCSD(T)/6-311G(2df)//QCISD/6-311G(d)+ZPVE level, the global minimum is the quasi-linear structure PCCCO **1** (0.0 kcal/mol) with a great kinetic stability of 47.9 kcal/mol, and the cumulenic form $\dot{P}=C=C=C=\bar{O}$ features largely in its resonance structures. Moreover, the chainlike isomer OPCCC **3** (64.5) and five-membered-ring species cPCCCO **19** (77.8) possess considerable kinetic stability of about 18.0 kcal/mol. All these three isomers are very promising candidates for future experimental and astrophysical detection. Additionally, a three-membered-ring isomer CCcCOP **10** (69.6) has slightly lower kinetic stability of around 15 kcal/mol and may also be experimentally observable. Possible formation mechanisms of the four stable isomers in interstellar space are discussed. The present research is the first attempt to study the isomerization and dissociation mechanisms of PC_nO series. The predicted spectroscopic properties, including harmonic vibrational frequencies, dipole moments and rotational constants for the relevant isomers, are expected to be informative for the identification of PC_3O in laboratory and interstellar medium.

Keywords Theoretical calculations · Structure · Stability · Potential energy surface (PES) · PC_3O

Y. Liu · X.-R. Huang (✉) · G.-T. Yu · H.-L. Liu · C.-C. Sun
State Key Laboratory of Theoretical and Computational Chemistry, Institute of Theoretical Chemistry, Jilin University, Changchun 130023, People's Republic of China
Tel.: +86-43-18498951
Fax: +86-43-18945942
E-mail: quanchemly@yahoo.com.cn

1 Introduction

Phosphorus and oxygen chemistry have received considerable attention from various fields. One particular interest is the possible role in astrophysical chemistry. It is well known that with the rapid development of spectrometric detective techniques, more than 120 species have so far been identified in interstellar and circumstellar dust clouds [1]. Among them, many phosphorus- or oxygen-containing molecules have been detected, such as C_nO (n=1, 2, 3, 5), CP, PN, NO, SO and CH_3CH_2OH [2]. Moreover, extensive experimental and theoretical investigations have been performed on the larger C_nO [2] and C_nP species [2–7]. The mixed PC_nO species may present a bridge between the C_nP and C_nO clusters and should be of astronomical interest. Understanding the properties of the structure, bonding and stability of PC_nO clusters may be helpful for future identification of new P, C and O-containing species either in the laboratory or in interstellar space and also for the elucidation of the formation mechanism of P-doped C_nO clusters or O-doped C_nP clusters. In particular, it is well known that the C_2P and C_3P species may exist in the molecular hot core of star-forming regions provided oxygen atoms are not injected [8]. On the contrary, if they are reactive with oxygen atoms, it is reasonable for us to speculate that many PC_2O and PC_3O isomers will be generated. Here we choose the PC_3O radical as our research object.

On the other hand, it should be mentioned that the analogous NC_nO [9] and NC_nS [10,11,13] clusters have obtained a large number of experimental and theoretical studies. Despite their potential importance, the PC_nO series has received little attention. Naturally, it should receive the same attention. In this paper, we study the penta-atomic PC_3O radical, which is the isoelectronic analogue of the NC_3S radical. Very recently, theoretical studies on the NC_3S radical showed that six chainlike isomers and three three-membered-ring species have considerable kinetic stability and may be observable in the laboratory [11]. It is worth noting that the predicted linear species NCCCS has been characterized by experiments [12,13]. Therefore, it is very possible that various kinetically

stable PC_3O isomers could be located on the potential energy surface (PES), just like the situation of NC_3S. On the other hand, the second-row elements P and S are well known to have a much less trend to form π-bonding than the corresponding first-row elements N and O. So there should be some difference in the structure, bonding and stability between PC_3O and NC_3S. In view of the rather limited knowledge of the important PC_3O radical, we decided to perform a detailed theoretical study on its PES, which is very significant for predicting the promising species to be detected.

In this paper, we are going to resolve the following four problems: (1) Is the chainlike PCCCO the ground state structure of the PC_3O radical just like NCCCS? (2) Are there any other chainlike species which are kinetically stable enough to be detected in the laboratory or interstellar space? (3) Does PC_3O have cyclic or cagelike isomers which are kinetically stable? (4) What is the nature of bonding in the relevant isomers?

2 Theoretical computational methods

All computations are carried out using the GAUSSIAN 98 [14] and MOLCAS 6.0 [15] (for CASSCF and CASPT2) program packages. The optimized geometries and harmonic vibrational frequencies of the isomers and transition states are initially obtained at the DFT/B3LYP/6-311G(d) level. To get reliable energies, the CCSD(T)/6-311G(2d) single-point energy calculations are performed based on the optimized geometries at the B3LYP/6-311G(d) level. The zero-point vibrational energies (ZPVE) at the B3LYP/6-311G(d) are also included for energy correction. The total CCSD(T)/6-311G(2d)//B3LYP/6-311G(d)+ZPVE is simplified as CCSD(T)//B3LYP. To confirm the right connective relationship between the isomers and transition states, we perform the intrinsic reaction coordinate (IRC) calculations at the B3LYP/6-311G(d) level. Furthermore, for the relevant isomers, the structures and frequencies are refined at the QCISD/6-311G(d) level and the energies are obtained at the CCSD(T)/6-311G(2df)//QCISD/6-311G(d)+ZPVE level [simplified as CCSD(T)//QCISD]. Finally, the CASSCF (11,10)/aug-cc-pVDZ structure optimization followed by CASPT2/aug-cc-pVDZ single-point energy calculation is performed for the relevant isomers to investigate the multiconfigurational effect [simplified as CASPT2//CASSCF]. We also performed the frequency analysis calculation using the MCKINLEY and MCLR programs of the MOLCAS 6.0 program system.

3 Results and discussion

To include as many isomers as possible, we initially considered six types of isomers: (I) linear or chainlike species, (II) three-membered-ring species, (III) four-membered-ring species, (IV) five-membered-ring species, (V) cagelike species and (VI) branched-chain species.

After an exhaustive search, a total of 29 minima (**m**) connected by 65 interconversion transition states (**TSm/n**) were located and their optimized geometries are shown in Figs. 1 and 2, respectively. Moreover, the optimized dissociation fragments of the PC_3O radical are shown in Fig. 3. The calculated spectroscopic properties of the relevant species, including harmonic vibrational frequencies, dipole moments and rotational constants, are listed in Table 1. And the relative energies of all isomers and transition states on different levels are given in Table 2. The relative energies of various dissociation fragments of PC_3O are collected in Table 3. Finally, the schematic PES of PC_3O radical is shown in Fig. 4. The most plausible pathways involving the lowest energy isomers are shown in Fig. 5.

3.1 PC_3O isomers

On the PES of PC_3O radical, eight isomers have chainlike structures and they are PCCCO **1** (0.0, 0.0, 0.0), CCPCO **2** (41.7), OPCCC **3** (63.0, 64.5, 72.3), CPCCO **4** (82.7), PCOCC **5** (101.8), POCCC **6** (103.2), POCCC **6′** (108.4) and PCCOC **7** (116.7). Note that the first, second, and third values in parentheses are obtained at the CCSD(T)//B3LYP, CCSD(T)//QCISD and CASPT2//CASSCF levels, respectively, and these values are relative with reference to isomer **1** (0.0, 0.0, 0.0). Among them, six isomers **2**, **3**, **4**, **5**, **6** and **7** are bent forms, whereas the two remaining species **1** and **6′** are quasi-linear and linear structures, respectively. The present B3LYP/6-311G(d) method predicts that the lowest-lying isomer PCCCO **1** (0.0, 0.0, 0.0) is the linear form with the lowest bending vibrational mode of about 85 cm^{-1}. Its highest occupied molecular orbital is a singly occupied π-orbital, giving rise to $a^2\Pi$ electronic state. However, the higher QCISD/6-311G(d) method predicts that the linear PCCCO structure has an imaginary frequency (117 i cm^{-1}). Once we relax the $C_{\infty v}$ symmetry, a slightly bent structure with ^{2} A″ electronic state is obtained with the lowest vibrational frequency of 72 cm^{-1}. The above phenomenon may be caused by the Renner–Teller effect. However, both the $C_{\infty v}$ and C_s symmetry optimizations of species **1** at the CASSCF level have all real frequencies, which indicates that the Renner–Teller effect could be small. Indeed, the obtained geometry parameters at B3LYP, QCISD and CASSCF methods are very close, as shown in Fig. 1.

For the three-membered-ring structure, six isomers are located as minima. They are OC-cCCP **8** (33.2), PC-cCCO **9** (63.9), CC-cCOP **10** (68.7, 69.6, 73.1), OP-cCCC **11**(71.3), PO-cCCC **12** (99.3) and P-cCOC-C **13** (105.8). Among them, four isomers **8**, **9**, **10** and **12** have the CCP ring with exocyclic OCC bonding, CCO ring with exocyclic PCC bonding, COP ring with exocyclic CCC bonding and CCC ring with exocyclic POC bonding, respectively, as shown in Fig. 1. All the four isomers have the same electronic state of ^{2} A″. Note that isomer **11** has an enantiomeric mirror image, and both of them have a CCC ring with exocyclic OPC bonding. The isomer **13** has a branched COC ring with two exocyclic CP and CC bondings.

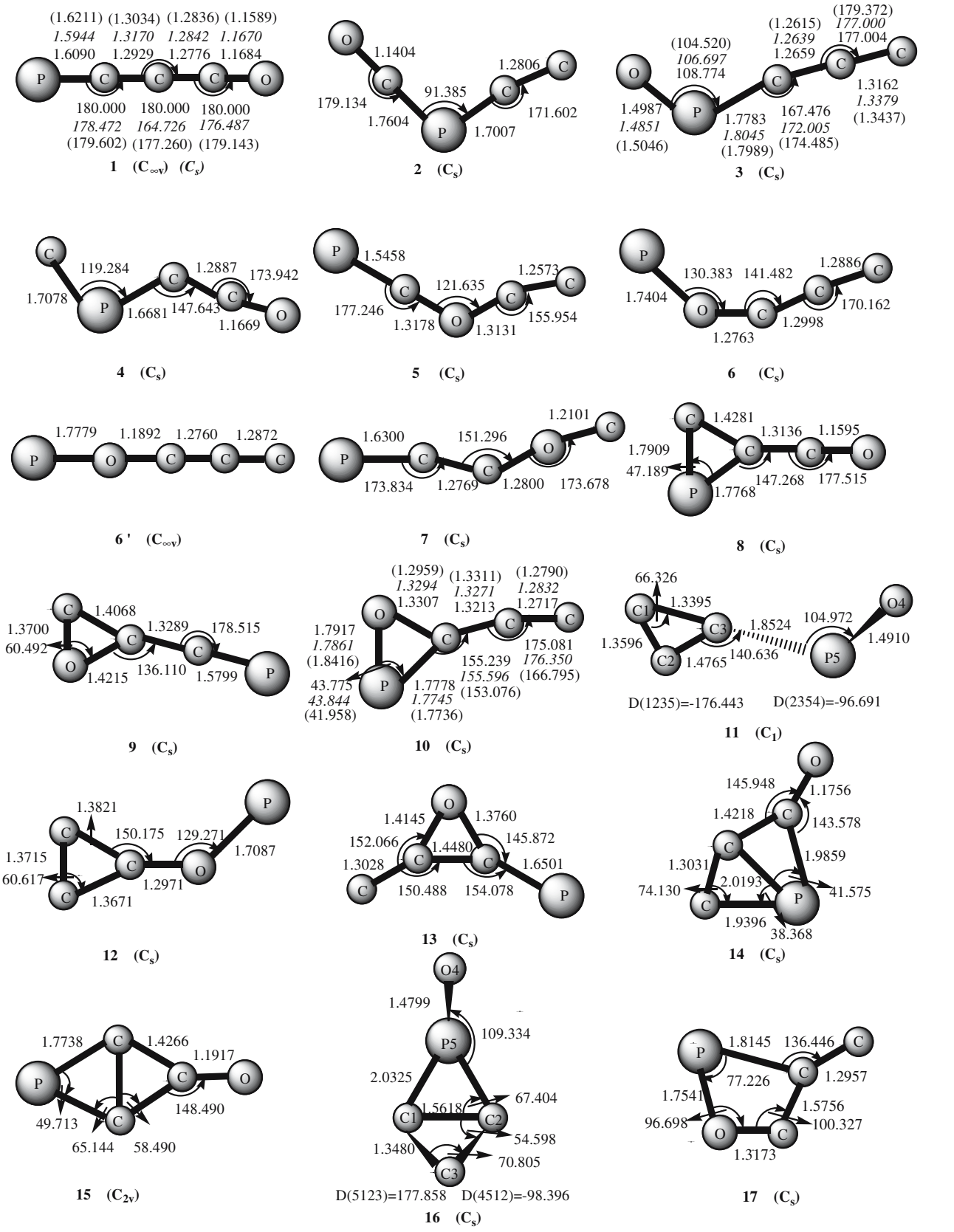

Fig. 1 Optimized geometries of doublet PC_3O isomers and the stable quartet structures at the B3LYP/6-311G(d) level. Bond lengths are in angstroms and angles are in degrees. The values in *italics* are at the QCISD/6-311G(d) level, and those in *parentheses* are at the CASSCF/aug-cc-pVDZ level

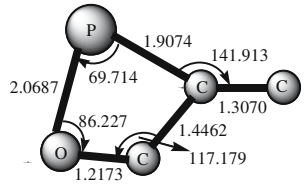

17 ' **(C_s)**

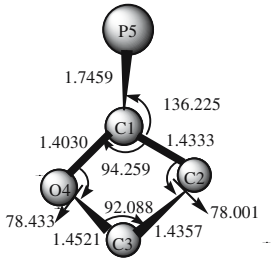

D(1234)=30.096 D(3215)=132.427

18 **(C_1)**

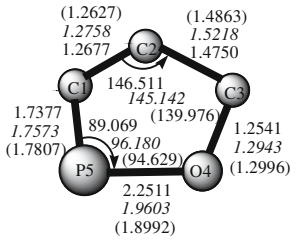

19 **(C_s)**

D(5123)=0.034 D(1234)=-0.032 ***(C1)***

(D(5123)=-0.022) (D(1234)=0.022) *(C1)*

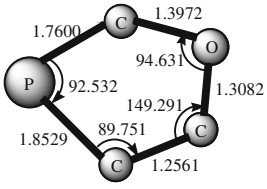

20 **(C_s)**

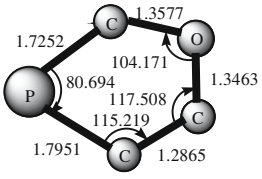

20 ' **(C_s)**

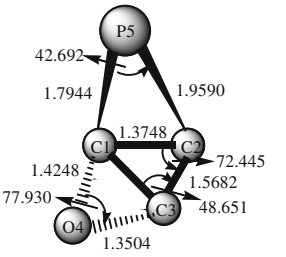

D(1234)=22.102 D(1235)=-53.614

21 **(C_1)**

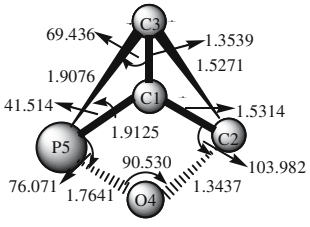

D(5124)=25.532 D(5123)=-71.583

22 **(C_1)**

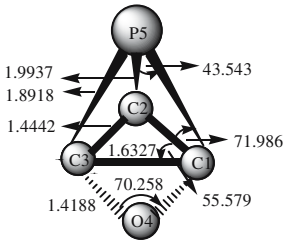

D(1234)=-27.907 D(1235)=70.897

23 **(C_s)**

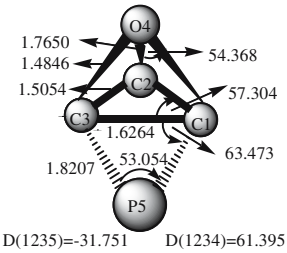

D(1235)=-31.751 D(1234)=61.395

24 **(C_s)**

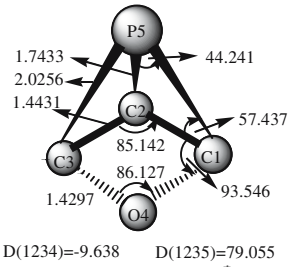

D(1234)=-9.638 D(1235)=79.055

25 **(C_s)**

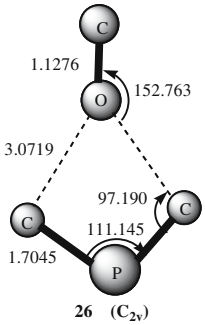

26 **(C_{2v})**

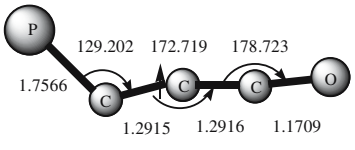

^{4}1 **(C_s)**

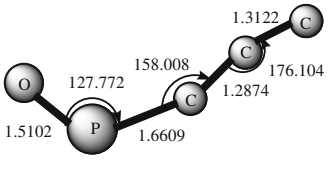

^{4}3 **(C_s)**

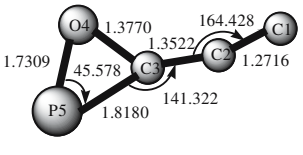

D(1234)=60.506 D(2345)=136.856

^{4}10 **(C_1)**

Fig. 1 (Contd.)

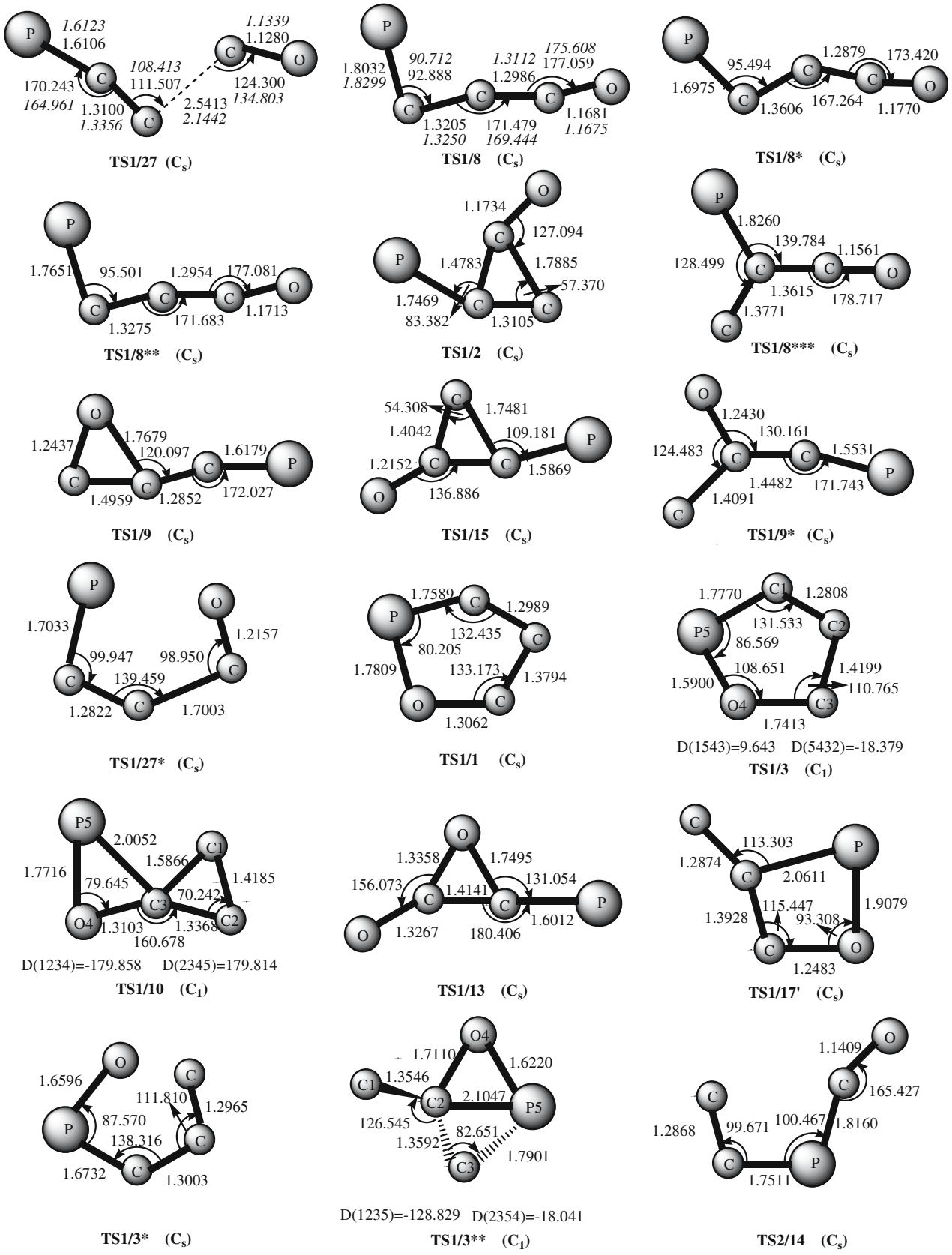

Fig. 2 Optimized geometries of PC_3O doublet transition states at the B3LYP/6-311G(d) level. Bond lengths are in angstroms and angles are in degrees. The values in *italics* are at the QCISD/6-311G(d) level

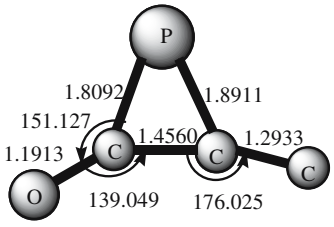

TS2/14* (C_s)

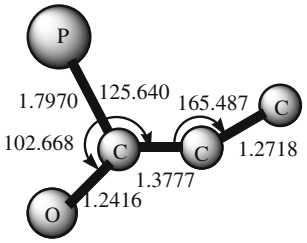

TS2/10 (C_s)

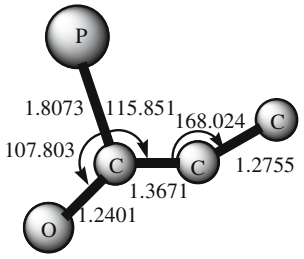

TS2/10* (C_s)

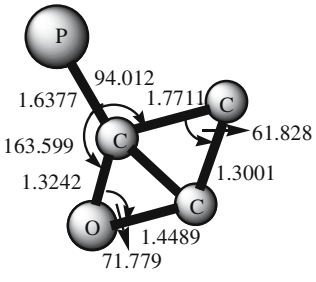

TS2/13 (C_s)

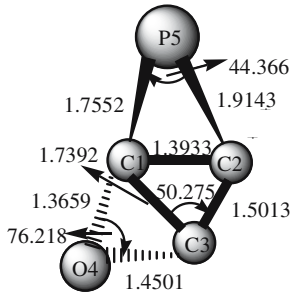

D(1234)=21.000 D(5123)=136.099
TS2/21 (C_1)

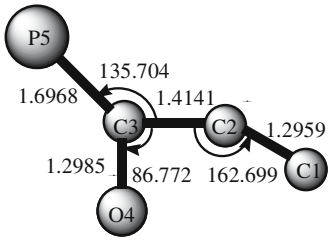

D(2345)=-179.997 D(1234)=0.002
TS2/13* (C_1)

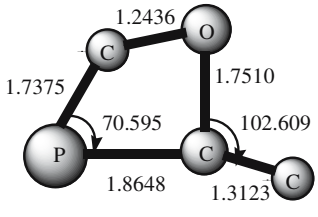

TS2/20 (C_s)

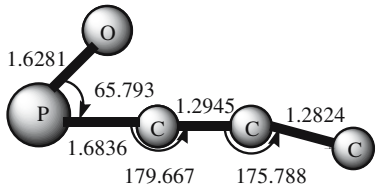

TS3/10 (C_s)

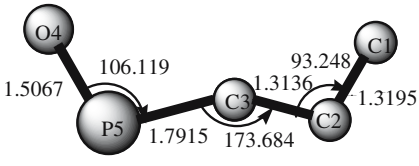

D(4532)=160.719 D(1235)=142.447
TS3/11 (C_1)

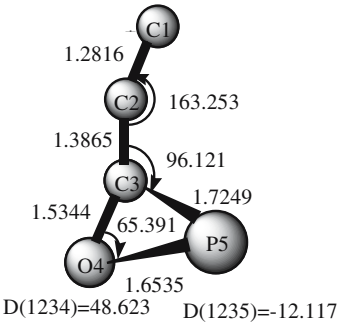

D(1234)=48.623 D(1235)=-12.117
TS3/14 (C_1)

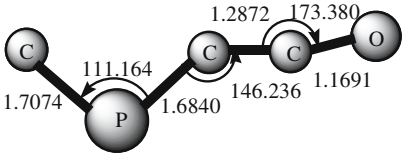

TS4/8 (C_s)

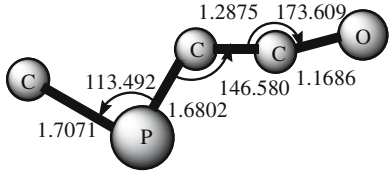

TS4/8* (C_s)

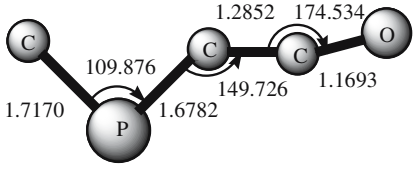

TS4/8 (C_s)**

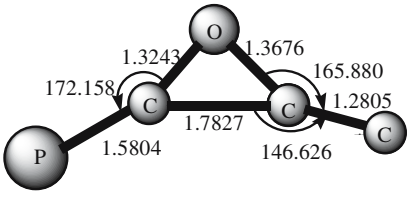

TS5/13 (C_s)

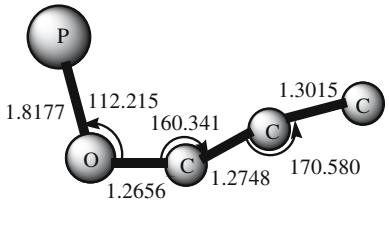

TS6/10 (C_s)

Fig. 2 (Contd.)

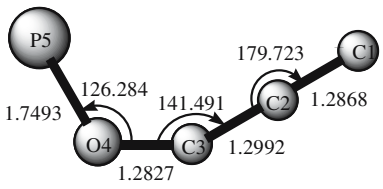

D(5432)=0.011 D(4321)=-90.383

TS6/6 (C_1)

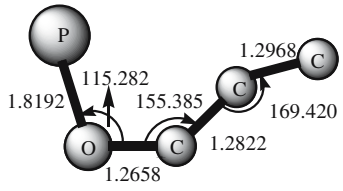

TS6/10* (C_s)

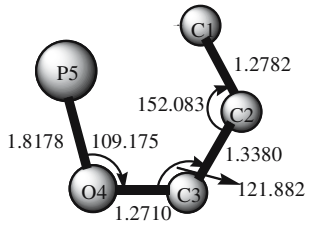

D(5432)=6.800 D(4321)=-9.689

TS6/19 (C_1)

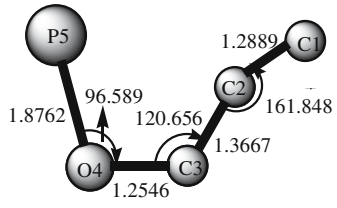

D(1234)=-149.560 D(2345)=-0.644

TS6/17 (C_1)

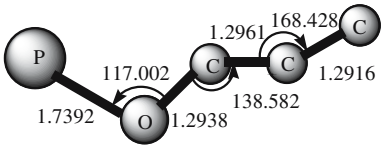

TS6'/10 (C_s)

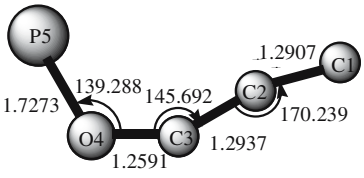

D(4321)=-179.911 D(5432)=-34.472

TS6'/6' (C_1)

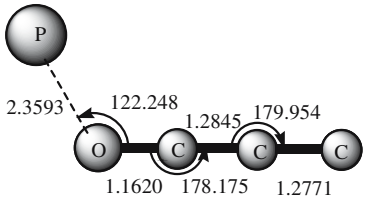

TS6'/10* (C_s)

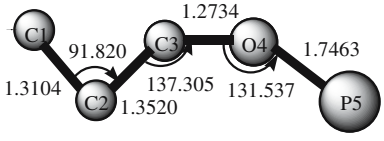

D(1234)=-160.637 D(2345)=-8.689

TS6'/12 (C_1)

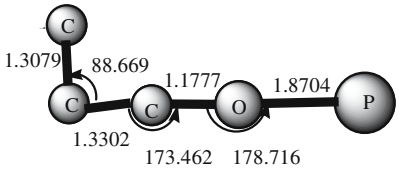

TS6'/12* (C_s)

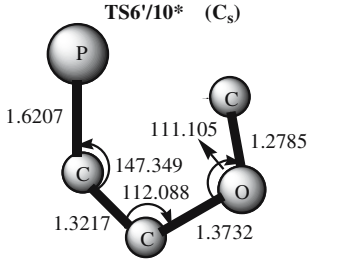

TS7/20' (C_s)

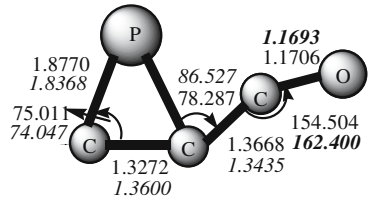

TS8/14 (C_s)

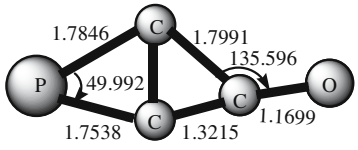

TS8/15 (C_s)

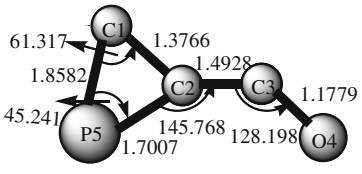

D(1523)=179.968 D(5234)=0.040

TS8/8 (C_1)

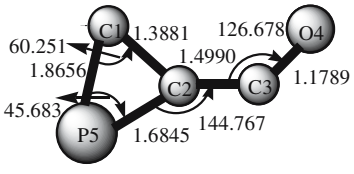

D(1523)=-179.953 D(5234)=179.943

TS8/8* (C_1)

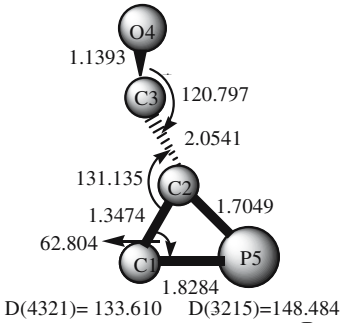

D(4321)= 133.610 D(3215)=148.484

TS8/27' (C_1)

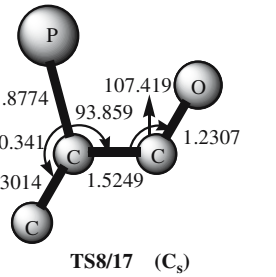

TS8/17 (C_s)

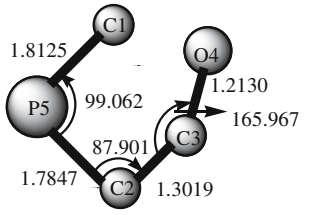

D(1523)=-12.451 D(5234)=17.303

TS8/20 (C_1)

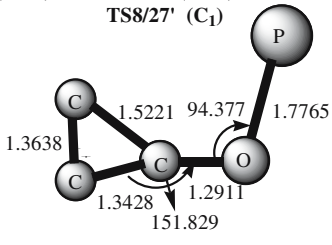

TS10/12 (C_s)

Fig. 2 (Contd.)

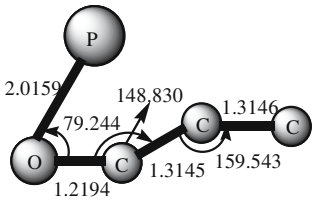

TS10/17' (C_s)

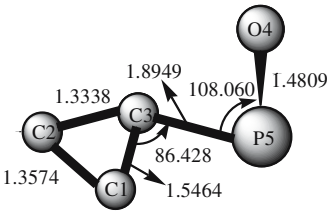

D(1235)=-1.568 D(2354)=-100.682

TS11/16 (C_1)

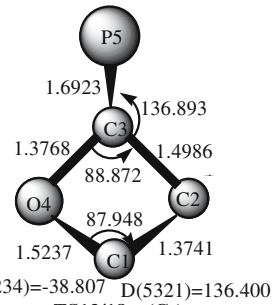

D(1234)=-38.807 D(5321)=136.400

TS13/18 (C_1)

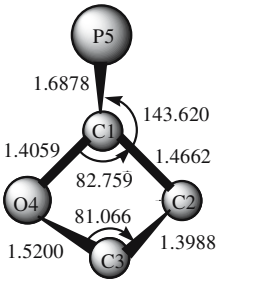

D(5143)=-138.772 D(1432)=-37.248

TS13/18* (C_1)

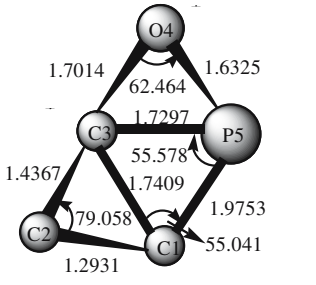

D(1234)=-67.245 D(2345)=105.794

TS14/16 (C_1)

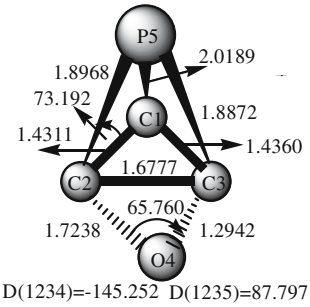

D(1234)=-145.252 D(1235)=87.797

TS14/23 (C_1)

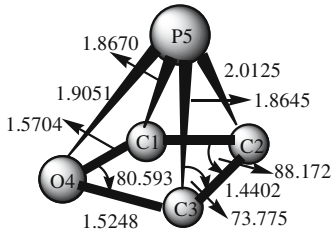

D(1234)=4.002 D(2345)=-69.463

TS14/25 (C_1)

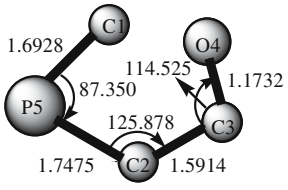

D(1523)=-7.385 D(5234)=14.036

TS15/20 (C_1)

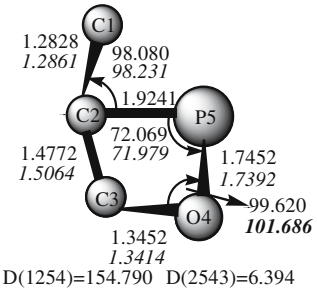

D(1254)=154.790 D(2543)=6.394

TS17/19 (C_1) (*Cs*)

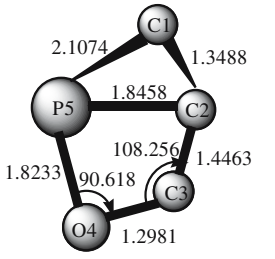

D(1523)=82.948 D(5234)=9.440

TS19/22 (C_1)

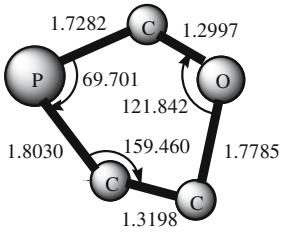

TS20/20' (C_s)

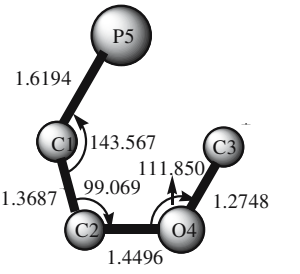

D(5124)=27.767 D(1243)=-21.395

TS20'/27 (C_1)

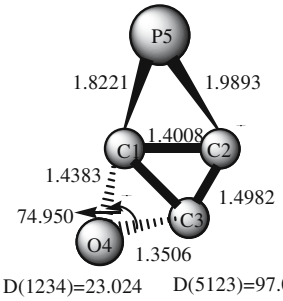

D(1234)=23.024 D(5123)=97.052

TS21/23 (C_1)

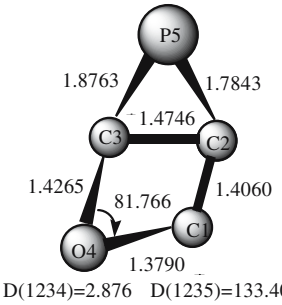

D(1234)=2.876 D(1235)=133.405

TS21/21 (C_1)

Fig. 2 (Contd.)

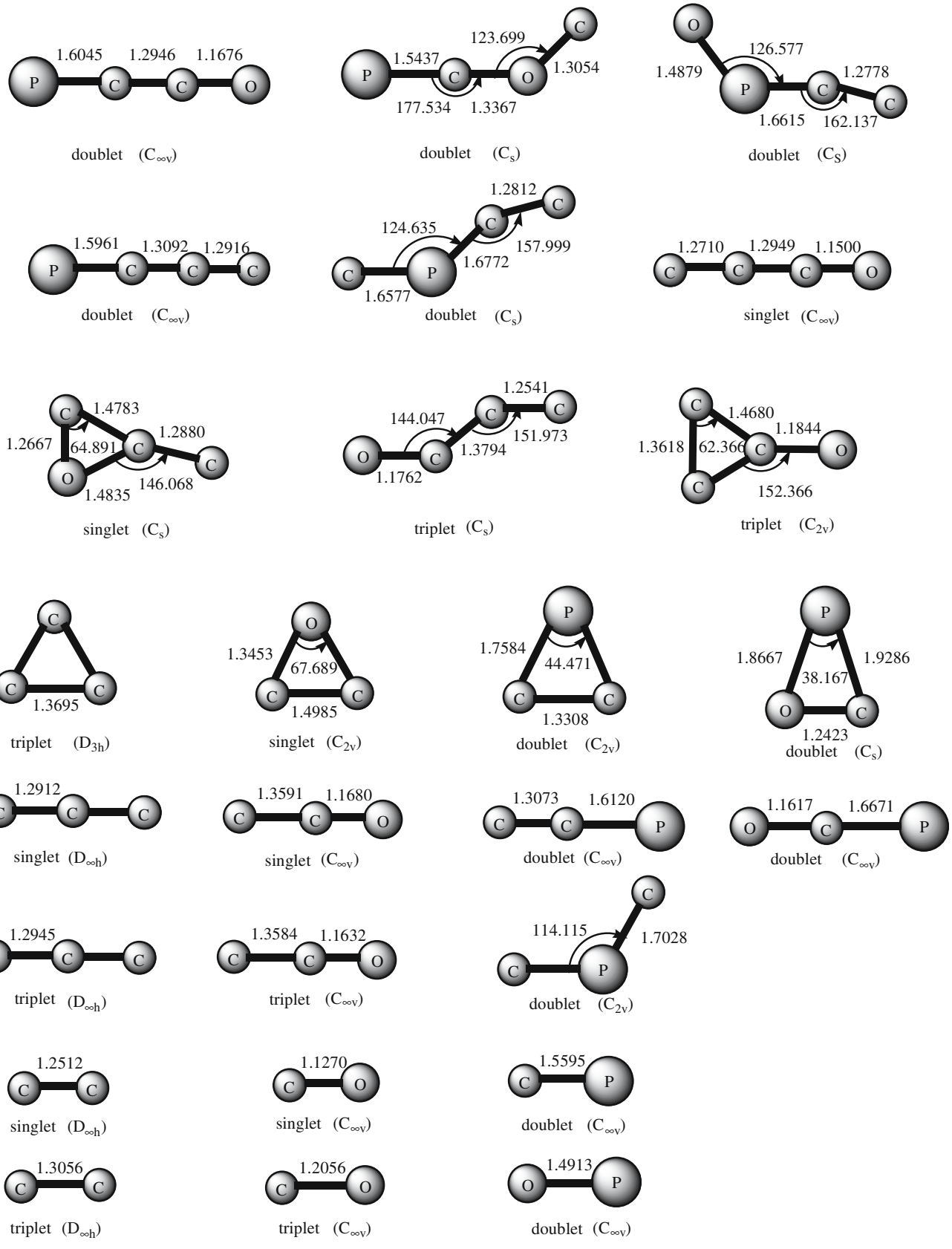

Fig. 3 Optimized fragments of the dissociations of PC_3O at the B3LYP/6-311G(d) level Bond lengths are in angstroms and angles are in degrees

Table 1 Harmonic vibrational frequencies (cm^{-1}), infrared intensities (km/mol) (in parentheses), dipole moment (D) and rotational constants (GHz) of the relevant doublet PC_3O structures at the B3LYP/6-311G(d) level

Species	Frequencies (infrared intensity)	Dipole moment	Rotational constant		
PCCCO **1**	85 (1), 120 (0), 388 (2), 413 (0), 507 (22), 577 (15), 585 (0), 1,204 (96), 1,826 (16), 2,258 (1,977)	0.8223	1.385		
PCCCO **1**[a]	72 (2), 325 (3), 424 (3), 537 (39), 557 (25), 606 (5), 1,214 (109), 1,753 (92), 2,254 (2,296)	0.7884	573.027	1.394	1.390
PCCCO **1**[b]	108 (0), 303 (0), 344 (0), 504 (32), 586 (17), 592 (9), 1,194 (99), 1,807(82), 2,238 (2,630)	0.0776	21,184.047	1.373	1.373
POCCC**3**	73 (7), 96 (1), 197 (3), 353 (7), 412 (3), 590 (79), 1,147 (86), 1,294 (89),1,968 (234)	2.0075	30.013	1.896	1.783
POCCC**3**[a]	56 (0), 94 (8), 239 (12), 325 (5), 416 (22), 596 (136), 1,229 (82), 1,264 (202), 1,957 (43)	2.4195	27.620	1.897	1.775
POCCC **3**[b]	104 (0), 111 (9), 263 (5), 370 (4), 443 (6), 595 (164), 1,160 (47), 1,281 (309), 1,951 (28)	2.1621	25.539	1.925	1.790
cPCCCO **19**	88 (8), 256 (8), 321 (1), 428 (5), 601 (25), 668 (17), 801 (85), 1,412 (166), 1,765 (30)	2.0021	9.412	5.003	3.267
cPCCCO **19**[a]	219 (2), 264 (17), 474 (1), 536 (3), 599 (23), 744 (14), 848 (85), 1,288 (31), 1,789 (9)	2.1495	9.071	5.834	3.551
cPCCCO**19**[b]	280 (4), 337 (7), 386 (6), 410 (50), 768 (61), 785 (10), 903 (103), 1,355 (63), 1,914 (5)	2.2313	8.822	6.108	3.609
CC-cCOP**10**	149 (8), 151 (3), 422 (2), 462 (3), 569 (23), 635 (37), 964 (73), 1,473 (107), 2,079 (984)	5.6532	18.081	2.598	2.271
CC-cCOP**10**[a]	130 (4), 144 (2), 429 (2), 439 (5), 594 (64), 645 (17), 1,020 (65), 1,486 (113), 2,052 (1,174)	5.7433	18.360	2.576	2.259
CC-cCOP**10**[b]	115 (3), 150 (7), 413 (1), 514 (8), 590 (83), 680 (6), 1,114 (60), 1,578 (276), 2,119 (1,620)	6.4797	16.383	2.664	2.291

For the relevant isomers, the QCISD/6-311G(d), CASSCF/aug-cc-pVDZ values are also included
[a] At the QCISD/6-311G(d) level
[b] At the CASSCF/aug-cc-pVDZ level

Table 2 Relative energies (kcal/mol) of the PC_3O structures and transition states at the B3LYP/6-311G(d) and single-point CCSD(T)/6-311G(2d) levels

Species	State	B3LYP[a]	Δ ZPVE B3LYP[a]	CCSD(T)[b] //B3LYP[a]	Total 1	QCISD[a]	Δ ZPVE QCISD[a]	CCSD(T)[c] //QCISD[a]	Total 2	Δ ZPVE CASSCF[d]	CASPT2// CASSCF[d]	Total 3
PCCCO 1[e]	$^2\Pi$	0.0	0.0	0.0	0.0	0.0	0.0	0.0	0.0	0.0	0.0	0.0
CCPCO 2	^{2} A″	55.2	−1.9	43.6	41.7							
OPCCC 3	^{2} A″	78.2	−2.6	65.6	63.0	70.9	−2.2	66.7	64.5	−2.1	74.4	72.3
CPCCO 4	^{2} A″	91.4	−2.1	84.8	82.7							
PCOCC 5	^{2} A′	117.8	−1.7	103.5	101.8							
POCCC 6	^{2} A″	113.3	−2.6	105.8	103.2							
POCCC 6′	$^2\Pi$	110.1	−1.9	110.3	108.4							
PCCOC 7	^{2} A′	116.7	−2.2	118.9	116.7							
OC-cCCP 8	^{2} A″	41.2	−1.0	34.2	33.2							
PC-cCCO 9	^{2} A″	74.6	−2.0	65.9	63.9							
CC-cCOP 10	^{2} A″	81.4	−1.5	70.2	68.7	73.1	−1.1	70.7	69.6	−0.7	73.8	73.1
OP-cCCC 11		90.5	−2.8	74.1	71.3							
PO-cCCC 12	^{2} A″	111.1	−2.0	101.3	99.3							
P-cCOC-C 13	^{2} A′	118.4	−2.2	108.0	105.8							
O-cCCCP 14	^{2} A″	55.7	−1.5	42.7	41.2							
O-cCCPC 15	^{2} B_1	52.8	−1.2	43.1	41.9							
O-cPCCC 16	^{2} A′	93.0	−2.5	75.3	72.8							
C-cCCOP 17	^{2} A″	112.0	−2.7	96.0	93.3							
C-cCCOP 17′	^{2} A′	128.2	−2.2	116.0	113.8							
P-cCCCO 18		141.7	−3.1	131.0	127.9							
cPCCCO 19	^{2} A″	93.6	−2.3	81.8	79.5	83.0	−1.4	79.2	77.8	−0.9	86.3	85.4
cPCOCC 20	^{2} A′	118.8	−1.4	105.3	103.9							
cPCOCC 20′	^{2} A′	121.4	−1.2	109.0	107.8							
cPCCOC 21		133.9	−2.2	119.0	116.8							
cageCCCOP 22		126.2	−1.5	110.8	109.3							
cagePCCOC 23	^{2} A′	128.4	−1.7	113.1	111.4							
cagePCCOC 24	^{2} A′	143.3	−2.6	125.4	122.8							
cagePCCOC 25	^{2} A″	143.3	−1.9	127.4	125.5							
C-cO ··· CPC 26	^{2} A_2	153.2	−5.2	127.3	122.1							
PCC+CO 27 [f]		63.1	−3.9	44.4	40.5							
cPCC+CO 27′ [f]		72.5	−4.4	52.5	48.1							
CPC+CO 27″ [f]		154.1	−5.5	128.7	123.2							
TS1/27	^{2} A″	62.6	−3.4	44.6	41.2	45.1	−3.0	50.9	47.9			
TS1/8	^{2} A″	63.8	−2.1	60.1	58.0	59.3	−1.7	60.2	58.5			
TS1/8*[g]	^{2} A″	65.9	−2.2	63.9	61.7							
TS1/8**	^{2} A″	65.9	−2.0	64.5	62.5							
TS1/2	^{2} A″	78.6	−2.2	67.7	65.5							
TS1/8***	^{2} A″	81.8	−2.3	71.5	69.2							
TS1/9	^{2} A″	81.5	−3.2	75.2	72.0							
TS1/15	^{2} A″	86.0	−2.7	76.8	74.1							
TS1/9*	^{2} A″	90.8	−2.5	77.8	75.3							
TS1/27*	^{2} A″	95.0	−3.0	78.8	75.8							
TS1/1	^{2} A′	102.0	−2.0	90.2	88.2							
TS1/3		120.6	−3.3	104.3	101.0							
TS1/10		120.7	−2.7	105.4	102.7							
TS1/13	^{2} A′	127.2	−2.9	117.3	114.4							
TS1/17′	^{2} A′	129.7	−1.3	118.5	117.2							
TS1/3*	^{2} A′	140.3	−2.6	126.9	124.3							
TS1/3**		152.2	−3.6	135.9	132.3							
TS2/14	^{2} A″	69.5	−2.6	54.2	51.6							
TS2/14*	^{2} A″	67.4	−2.0	57.7	55.7							
TS2/10	^{2} A″	103.3	−2.6	93.9	91.3							
TS2/10*	^{2} A″	103.7	−2.4	97.8	95.4							
TS2/13	^{2} A′	134.4	−2.7	120.1	117.4							
TS2/21		135.1	−2.6	122.8	120.2							
TS2/13*		136.6	−3.0	127.7	124.7							
TS2/20	^{2} A′	143.7	−1.4	132.0	130.6							
TS3/10	^{2} A″	96.5	−2.6	86.1	83.5	92.6	−2.8	86.2	83.4			

Table 2 (Contd.)

TS3/11		103.5	−3.3	88.2	84.9				
TS3/14		130.7	−2.8	118.6	115.8				
TS4/8	^{2} A″	93.0	−2.4	84.0	81.6				
TS4/8*	^{2} A″	92.9	−2.4	84.5	82.1				
TS4/8**	^{2} A″	91.5	−2.2	85.0	82.8				
TS5/13	^{2} A′	126.0	−2.8	116.3	113.5				
TS6/10	^{2} A″	115.8	−3.2	108.8	105.6				
TS6/6		120.1	−2.8	113.0	110.2				
TS6/10*	^{2} A″	121.2	−3.2	114.7	111.5				
TS6/19		129.4	−2.4	120.6	118.2				
TS6/17		130.6	−2.8	121.9	119.1				
TS6′/10	^{2} A″	114.3	−2.7	105.3	102.6				
TS6′/6′		113.5	−2.9	108.6	105.7				
TS6′/10*	^{2} A″	117.6	−1.8	108.8	107.0				
TS6′/12		136.7	−3.4	125.6	122.2				
TS6′/12*	^{2} A″	130.7	−2.7	125.6	122.9				
TS7/20′	^{2} A′	147.9	−1.6	134.0	132.4				
TS8/14	^{2} A″	56.1	−1.8	44.8	43.0				
TS8/15	^{2} A″	59.0	−1.9	49.7	47.8				
TS8/8		67.2	−1.9	53.6	51.7				
TS8/8*		69.8	−2.0	55.4	53.4				
TS8/27′		78.5	−3.4	62.8	59.4				
TS8/17	^{2} A″	123.4	−3.4	112.8	109.4				
TS8/20		130.7	−3.0	117.2	114.2				
TS10/12	2A″	125.3	−2.9	114.4	111.5				
TS10/17′	^{2} A′	138.9	−2.8	130.6	127.8				
TS11/16		93.4	−2.6	75.3	72.7				
TS13/18		148.2	−3.7	134.0	130.3				
TS13/18*		146.3	−3.9	134.6	130.7				
TS14/16		134.1	−2.8	62.0	59.2				
TS14/23		131.3	−2.3	116.8	114.5				
TS14/25		150.0	−3.2	132.2	129.0				
TS15/20		152.3	−4.0	128.6	124.6				
TS17/19		114.8	−2.8	98.6	95.8	102.0	−2.5	98.1	95.6
TS19/22		128.4	−2.2	112.6	110.4				
TS20/20′	^{2} A′	147.9	−3.0	133.7	130.7				
TS20′/27		140.5	−3.6	128.3	124.7				
TS21/23		135.2	−2.3	120.1	117.8				
TS21/21		150.2	−3.1	141.9	138.8				
PCCCO ^{4} 1	^{4} A″	46.0	−1.1	43.1	42.0				
OPCCC ^{4} 3	^{4} A″	108.0	−2.3	100.4	98.1				
CC-cCOP ^{4} 10		126.2	−2.8	115.7	112.9				

For the relevant isomers, the CCSD(T)/6-311G(2df)//QCISD/6-311G(d) and CASPT2/aug-cc-pVDZ//CASSCF/aug-cc-pVDZ values are also included

[a] The basis set is 6-311G(d) for B3LYP and QCISD

[b] The basis set is 6-311G(2d) for CCSD(T)

[c] The basis set is 6-311G(2df) for CCSD(T)

[d] The basis set is aug-cc-pVDZ and 11 electrons and 10 active orbitals are used for the CASSCF and CASPT2 methods

[e] The total energies of reference isomer **1**at the B3LYP/6-311G(d) level is −530.8587006 a.u., at the CCSD(T)/6-311G(2d)//B3LYP/6-311G(d) level is −529.9108931 au, at the QCISD/6-311G(d) level is −529.8253207 a.u., at the CCSD(T)/6-311G(2df)//QCISD/6-311G(d) level is −529.9923578 a.u., at the CASPT2/aug-cc-pVDZ//CASSCF/aug-cc-pVDZ level is −529.8105754 a.u. The ZPVE at the B3LYP, QCISD and CASSCF levels are 11.38434, 11.06832, 11.12 kcal/mol, respectively

[f] The **27**,**27′**, **27″** are the dissociation fragments PCC(^{2}¶)+CO($^1\Sigma$), cPCC(^{2} B_2)+CO($^1\Sigma$) and CPC(^{2} A_2)+CO($^1\Sigma$), respectively

[g] The "*" is used for distinguishing the transition states correlating the same two isomers.

Six isomers possess four-membered-ring structures. They are O-cCCCP **14** (41.2), O-cCCPC **15** (41.9), O-cPCCC **16** (72.8), C-cCCOP **17** (93.3), C-cCCOP **17′** (113.8) and P-cCCCO **18** (127.9). Isomer **14** has a CCCP ring with CP cross-bonding and exocyclic CO bonding. Isomers **15** and **16** possess the same CCCP ring with CC cross-bonding; however, each isomer has different exocyclic bonding, i.e., respective CO and PO bondings. Different from the three isomers above, the remaining three four-membered-ring species do not have any cross-bondings. The isomers **17** and **17′** have the same atomic arrangements, but they belong to different electronic states of ^{2}A″ and ^{2}A′, respectively. Isomer **18** has a CCCO ring with exocyclic CP bonding.

There are four five-membered-ring isomers. The B3LYP method predicts that the isomer cPCCCO **19** (79.5, 77.8, 85.4) belongs to the C_s point group. However, its optimization of C_s symmetry at the QCISD level has an obvious imaginary frequency (314i cm^{-1}), then relaxation of the C_s

Table 3 Relative (kcal/mol) energies of dissociation fragments of the PC_3O structures at the B3LYP/6-311G(d) and single-point CCSD(T)/6-311G(2d) levels

Species	B3LYP[a]	Δ ZPVE B3LYP[a]	CCSD(T)[b]//B3LYP[a]	Total
$PCCO(^2\Pi)+C(^3P)$	147.9	−2.9	134.0	131.1
$PCOC(^2A')+C(^3P)$	237.3	−4.9	214.1	209.2
$OPCC(^2A')+C(^3P)$	219.1	−5.3	195.7	190.4
$PCCC(^2\Pi)+O(^3P)$	167.5	−3.9	153.3	149.4
$CPCC(^2A')+O(^3P)$	256.7	−5.7	237.2	231.5
$CCCO(^1\Sigma)+P(^2D)$	121.2	−1.6	107.4	105.8
$C\text{-}cCCO(^1A')+P(^2D)$	221.8	−4.0	202.8	198.8
$OCCC(^3A')+P(^2D)$	190.1	−3.7	176.0	172.3
$O\text{-}cCCC(^3B_2)+P(^2D)$	192.1	−2.7	177.3	174.6
$CCCO(^1\Sigma)+P(^4S)$	82.6	−1.6	64.5	62.9
$C\text{-}cCCO(^1A')+P(^4S)$	183.2	−4.0	159.9	155.9
$OCCC(^3A')+P(^4S)$	151.5	−3.7	133.2	129.5
$O\text{-}cCCC(^3B_2)+P(^4S)$	153.5	−2.7	134.4	131.7
$cCCC(^3A_1')+OP(^2\Pi)$	149.3	−4.0	131.7	127.7
$CCC(^1\Sigma_g)+OP(^2\Pi)$	130.2	−4.5	109.3	104.8
$CCC(^3\Pi_g)+OP(^2\Pi)$	180.4	−6.1	159.4	153.3
$cCOC(^1A_1)+CP(^2\Sigma)$	187.9	−4.8	165.1	160.3
$CCO(^1\Pi)+CP(^2\Sigma)$	168.9	−3.9	148.8	144.9
$CCO(^3\Sigma)+CP(^2\Sigma)$	143.8	−4.0	128.5	124.5
$PCC(^2\Pi)+CO(^1\Sigma)$	63.1	−3.9	44.4	40.5
$CPC(^2A_2)+CO(^1\Sigma)$	154.1	−5.5	128.7	123.2
$cPCC(^2B_2)+CO(^1\Sigma)$	72.5	−4.4	52.5	48.1
$PCC(^2\Pi)+CO(^3\Pi)$	199.4	−4.5	184.6	180.1
$CPC(^2A_2)+CO(^3\Pi)$	290.4	−6.2	269.0	262.8
$cPCC(^2B_2)+CO(^3\Pi)$	208.8	−5.1	192.7	187.6
$PCO(^2\Pi)+CC(^1\Sigma_g)$	173.3	−3.6	132.0	128.4
$cPCO(^2A'')+CC(^1\Sigma_g)$	229.8	−5.1	184.7	179.6
$PCO(^2\Pi)+CC(^3\Pi_u)$	150.6	−3.8	134.3	130.5
$cPOC(^2A'')+CC(^3\Pi_u)$	207.2	−5.4	187.0	181.6

The total energies of reference isomer **1** at the B3LYP and single-point CCSD(T) levels as well as the ZPVE at the B3LYP level are listed in the Footnote e of Table 2. The symbols in parentheses of the column denote the electronic states

[a] The basis set is 6-311G(d) for B3LYP

[b] The basis set is 6-311G(2d) for CCSD(T)

symmetry of the cyclic species **19** leads to a C_1 symmetry minimum with small dihedral angles, which is consistent with the results of CASSCF method, as shown in Fig. 1. Both five-membered-ring isomers, cPCOCC **20** (103.9) and cPCOCC **20′** (107.8), belong to C_s point group with $^2A'$ electronic state. Isomer cPCCOC **21** (116.8) is a cyclic three-dimensional structure with two CC cross-bondings.

Four isomers **22** (109.3), **23** (111.4), **24** (122.8) and **25** (125.5) may be described as interesting cagelike forms. Except for the isomer **22** belonging to the C_1 point group, the others all have C_s symmetry. Obviously, all the four cagelike isomers are very high-lying and kinetically unstable which will be introduced in the following section. Unsurprisingly, for such a small molecule involving only five atoms, the cagelike species is generally rather compact with acute bonding angles and few multiple bonds. Finally, the isomer **26** (122.1), which is a weakly bound complex between the CPC radical and the CO molecule, will directly dissociate to the corresponding fragments. The branched-chain species could not be located.

3.2 PC_3O isomerization and dissociation stability

To discuss the kinetic stability, one needs to consider as many isomerization and dissociation pathways as possible. The lowest dissociation or isomerization barrier governs the kinetic stability of an isomer. In general, with higher barrier, an isomer could have higher kinetic stability. For simplicity, we will give no details of the obtained 65 transition states. The relative energies of the dissociation fragments of PC_3O are shown in Table 3. On the PES of PC_3O, four isomers **1**, **3**, **19** and **10** attract much interest with relatively high kinetic stability. Interestingly, for species **1**, the lowest dissociation barrier 41.2 (*47.9*) (**1**→ **27**) is lower than the lowest isomerization barrier 58.0 (*58.5)* (**1**→ **8**); therefore, the former governs its kinetic stability. However, for the remaining three isomers **3**, **19** and **10**, the lowest isomerization barriers govern the kinetic stability of them, and the corresponding lowest isomerization barriers are as follows: 20.5 (*18.9*) (**3** → **10**), 16.3 (*17.8*) (**19**→ **17**) and 14.8 (*13.8*) (**10** → **3**) kcal/mol, respectively. Note that the italic values in parentheses are obtained at

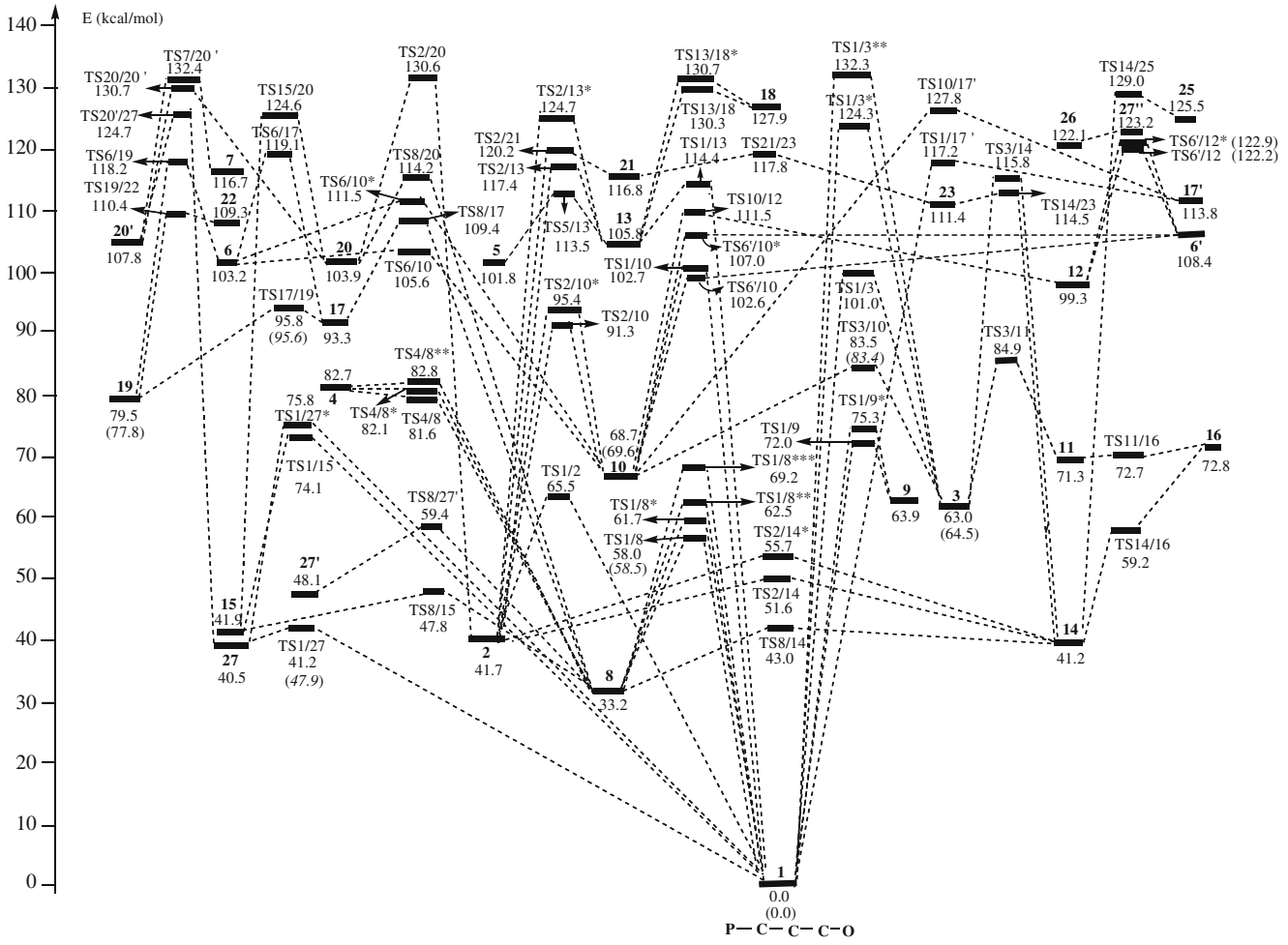

Fig. 4 Schematic potential energy surface of PC_3O at the CCSD(T)/6-311G(2d)//B3LYP/6-311G(d)+ZPVE level. The relative values in *parentheses* are at the CCSD(T)/6-311G(2df)//QCISD/6-311G(d)+ZPVE level

the CCSD(T)//QCISD level. Three isomers **1**, **3** and **19** with considerable kinetic stability are expected to be observable in the laboratory and in interstellar space. Compared with the three isomers **1**, **3** and **19**, the species **10** shows relatively lower kinetic stability. Such kinetic stability is high enough to allow its existence under low-temperature conditions such as dense interstellar clouds.

Apart from **1**, **3**, **19** and **10**, the other isomers generally have much lower kinetic stability due to the barrier energies of less than 10 kcal/mol or the high energies of themselves. As shown in Fig. 4, at the CCSD(T)//B3LYP level, the lowest barriers of the remaining species are 9.9 (**2**, **2** → **14**), −1.1 (**4**, **4** → **8**), 2.4 (**6**, **6** → **10**), −5.8 (**6′**, **6′** → **10**), 9.8 (**8**, **8** → **14**), 8.1 (**9**, **9** → **1**), 1.4 (**11**, **11** → **16**), 7.7 (**13**, **13** → **5**), 1.8 (**14**, **14** → **8**), 5.9 (**15**, **15** → **8**), −13.6 (**16**, **16** → **14**), 2.5 (**17**, **17** → **19**), 3.4 (**17′**, **17′** → **1**), 2.4 (**18**, **18** → **13**), 1.0 (**21**, **21** → **23**), 1.1 (**22**, **22** → **19**), 3.1 (**23**, **23** → **14**), 3.5 (**25**, **25** → **14**), 1.1 (**26**, **26** → **27″**), 11.7 (**5**, **5** → **13**), 15.7 (**7**, **7** → **20′**), 12.2 (**12**, **12** → **10**), 10.3 (**20**, **20** → **8**) and 16.9 (**20′**, **20′** → **27**) kcal/mol, respectively. For the latter five isomers**5**, **7**, **12**, **20** and **20′**, their lowest barrier energies lie between 10 and 17 kcal/mol and they seem to have moderate kinetic stability. However, they may not be detected in interstellar space because of their high-lying relative energies (about or more than 100 kcal/mol). In addition, several energy barriers mentioned above are negative, and it means those corresponding isomers are so unstable that they could convert to others easily. Despite many attempts, the transition state connecting with isomer **24** cannot be located. Nevertheless, species **24** is expected to be of little importance for the identification of PC_3O in experiment because of its high-lying energy (122.8 kcal/mol).

3.3 Properties and implications of the relevant isomers

From above, we know that four isomers **1**,**3**,**19** and **10** have higher kinetic stability and more possibilities to be detected by the experiment. In this section, we analyze their structural and bonding properties with the NBO (Natural Bond Orbital) analysis programs [16], mainly based on the B3LYP results.

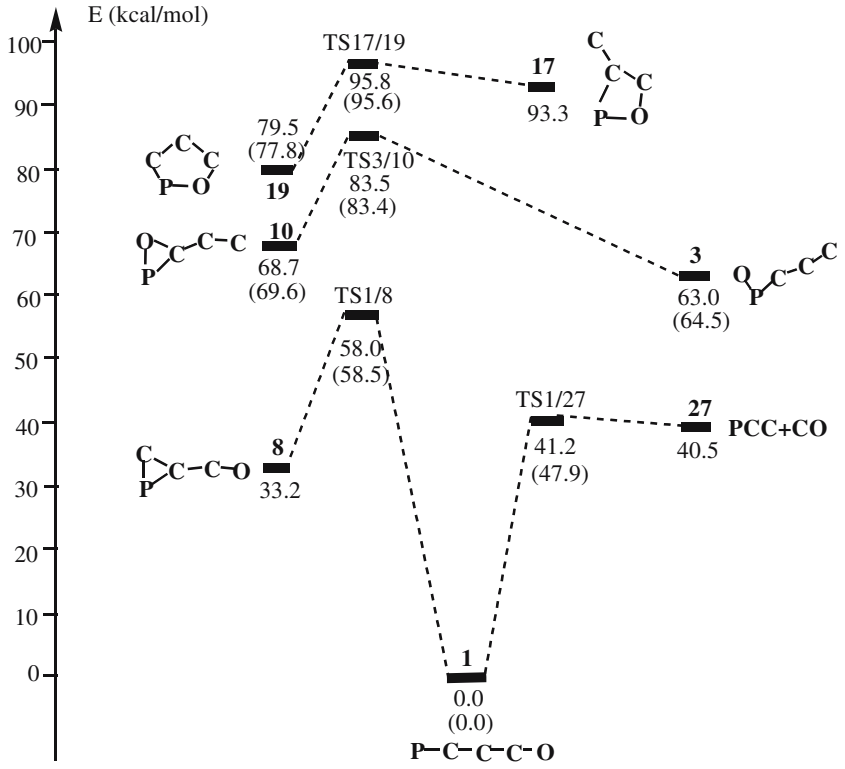

Fig. 5 Schematic potential energy surface of PC_3O including the most feasible pathways of the kinetically stable species at the CCSD(T)/6-311G(2d)//B3LYP/6-311G(d)+ZPVE level. The relative values in *parentheses* are at the CCSD(T)/6-311G(2df)//QCISD/6-311G(d) +ZPVE level

For the ground-state species PCCCO **1**, at the B3LYP/6-311G(d) level, its calculated PC bond length (1.6090 Å) lies between the typical P≡C triple bond (1.5395 Å in HC≡P [1]) and P=C double bond (1.6704 Å, see footnote 1). Similarly, the calculated two CC (1.2929 and 1.2776 Å) lengths and one CO (1.1684 Å) bond length also lie between their corresponding triple bond and double bond (see footnote 1). The spin density distribution is 0.600, −0.126, 0.359, 0.001 and 0.165e for P, C, C, C and O, respectively. With many references to the Wiberg bond index matrix, the species**1**may be described by the three resonance forms: (1) $\dot{\underline{P}} = C = C = C = \underline{O}$, (2) $\underline{P} \equiv C - \dot{C} = C = \underline{O}$, and (3) $\underline{P} \equiv C - C \equiv C - \underline{O}\bullet$, and their weights are degressive from (1) to (3). The symbols "•" and "-" represent the single electron and lone-pair electrons, respectively. Especially, the cumulenic form (1) should contribute largely to the stability of species **1**. It should be mentioned that for the analogous NC_3S radical [11], the relative weight order of the three resonant forms of ground-state NCCCS is just opposite as (1)<(2)<(3). The difference can be explained by the fact that C≡P triple bonding and C=S double bonding are much weaker than the corresponding C≡N bonding and C=O bonding, respectively.

For the bent OPCCC **3**, the spin density distribution is 0.190, −0.004, 0.411, −0.102 and 0.506 e for O, P, C, C, and C, respectively. Combined with the bond lengths shown in Fig. 1 and the Wiberg bond index matrix, we can express its resonance structures as follows:

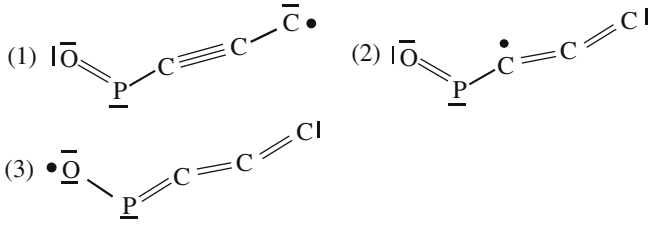

The weights of the three forms decrease from (1) to (3). The bent structure of species**3**may result from its internal P-atom. It is noticeable that the analogous SNCCC [11] is a linear form with $^2\Pi$ electronic state, which indicates that the p–p overlaps among nitrogen, carbon and sulfur are much more effective than that among phosphorus, carbon and oxygen. A similar situation also occurs between the bent isomer CCPCC [17] and the linear species CCNCC [18].

Isomer **19** has a five-membered-ring structure. Its spin density distribution (0.874, −0.146, 0.271, 0.007 and

[1] For parallel comparison, the bond distances C–P (1.8728 Å), C=P (1.6704 Å), C≡P (1.5395 Å), C–C (1.5308 Å), C=C (1.3270 Å), C≡C (1.1982 Å), C–O(1.4199 Å), C=O (1.2002 Å), C≡O (1.1271 Å), P–O (1.6797 Å), P=O (1.4939 Å), P≡O (1.4915 Å) are calculated at the B3LYP/6-311G(d,p) (p for H-atom) level, for the model systems CH_3PH_2, CH_2PH, CHP, CH_3CH_3, CH_2CH_2, CHCH, CH_3OH, CH_2O, CO, PH_2OH, PHO and PO, respectively.

−0.006 e for P, C, C, C and O, respectively) indicates that the single electron resides primarily on the P atom. Based on the bond lengths shown in Fig. 1, isomer **19**could be viewed as resonating between the following two structures:

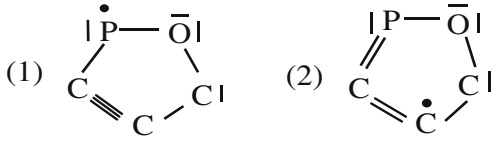

The form (1) has much more weight than (2). It should be mentioned that for NC_3S radical, no stable five-membered-ring isomer is reported [11].

The CC-cCOP **10** species has a three-membered-ring structure. Based on the bond lengths and the spin density distribution (0.904, 0.145, −0.038, 0.013, and −0.023 e for P, O, C, C and C, respectively), the species **10** can be viewed as having three resonant forms:

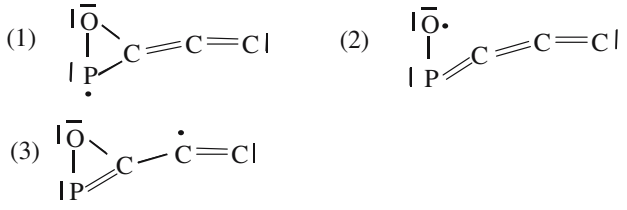

The distribution of spin density indicates the single electron is mainly localized on the P atom. So we give the highest priority to the first form.

3.4 Interstellar and laboratory implications

On the PES of PC_3O, three sets of dissociation products **27**, **27′**, **27″** attract much attention. It is well known that the C_2P species may exist in the molecular hot core of star-forming regions provided the oxygen atoms are not injected [8]. The CO molecule exists popularly in interstellar medium [1,2]. Therefore the association reaction between C_2P and CO is expected to produce the titled molecule PC_3O. From the PES, we can see that with a very small barrier of 0.7 kcal/mol, the linear CCP and CO can also lead to the products of species PCCCO **1**. It should be mentioned that the linear CCP was predicted to be ground state on the PES of C_2P. From energetic considerations, the formation of isomer **1** may easily occur under laboratory and interstellar conditions.

Up to now, many interstellar molecules with chainlike or cyclic structures have actually been reported. However, a cyclic phosphorus-containing species has not been detected in interstellar space. So we expect that the two cyclic species **10** and **19** could give good examples for experimental and interstellar detection. In order to identify the isomers of PC_3O better in the laboratory, the calculated vibrational frequencies, dipole moments and rotational constants for the four relevant isomers are shown in Table 1. At the QCISD/6-311G(d) level, the dominant frequencies of four isomers **1**, **3**, **19** and **10** are 2,254, 1,264, 848 and 2,052 cm^{-1}, with the corresponding infrared intensities 2,296, 202, 85 and 1,174 km/mol, respectively. They are very helpful for spectroscopic research on the PC_3O radical. Moreover, the isomers**3**, **19** and **10**have large dipole moments of 2.4195, 2.1495 and 5.7433 D, respectively, which are also a benefit for future microwave detection.

It is worth mentioning that for the four isomers (**1**, **3**, **19**, **10**) and relevant transition states (**TS1/8**, **TS1/27**, **TS3/10**, **TS17/19**), their calculated results at the B3LYP/6-311G(d) generally accord with those at higher QCISD/6-311G(d) level, as shown in Figs. 1, 2 and 3 and Tables 1 and 2. Furthermore, the CASPT2//CASSCF calculations are carried out to check the multiconfigurational properties of the above four relevant species, considering 10 frontier orbitals as active space and allowing 11 electrons to be excited within them, denoted as (11,10). The calculated relative energies, structures and spectroscopic values of the four species are close to the CCSD(T)//B3LYP and CCSD(T)//QCISD results. Especially, the leading electronic configurations occupied by **1**, **3**, **19** and **10** have come to 82.7, 83.3, 88.0, and 88.9%, respectively, at the CASSCF level. It indicates that the multiconfigurational effect could be ignored in PC_3O system and the CCSD(T)//B3LYP method is adequate for its calculation of the structures, energies and spectra. In addition, we also investigated the quartet species ^{4}**1**, ^{4}**3**, ^{4}**10** and ^{4}**19**(number **4** means quartet state) corresponding to the stable doublet isomers **1**, **3**, **10** and **19**, respectively. Note that the quartet isomer ^{4}**19** could not be located. The geometrical structures of the obtained quartet isomers are shown in Fig. 1. The computed results showed that quartet isomers ^{4}**1**, ^{4}**3** and ^{4}**10** are much higher in energy than the corresponding doublet species with large doublet–quartet energy gap of 42.0, 35.1 and 44.2 kcal/mol, respectively, at the CCSD(T)//B3LYP level. Thus the quartet PC_3O isomers were not considered further.

4 Summary

At the CCSD(T)//B3LYP, CCSD(T)//QCISD and CASPT2//CASSCF levels, the doublet PES of PC_3O radical is established, including 29 minimum isomers and 65 interconversion transition states. At the CCSD(T)// QCISD level, the quasi-linear isomer PCCCO **1**(0.0, 0.0, 0.0) has a great kinetic stability of 47.9 kcal/mol. Additionally, both bent isomer OPCCC **3**(63.0, 64.5, 72.3) and five-membered-ring species cPCCCO **19** (79.5, 77.8, 85.4) have considerable kinetic stability of around 18 kcal/mol. All three isomers could be produced under certain laboratory and interstellar conditions. In particular, the isomer **19** should represent an interesting cyclic phosphorus-containing radical in the laboratory or in interstellar space. Moreover, the three-membered-ring CC-cCOP**10** (68.7, 69.6, 73.1) with slightly lower kinetic stability is possible to observe. The present study is expected to help in the identification of PC_3O radical in the laboratory and in interstellar space.

Acknowledgements This work is supported by the National Nature Science Foundation of China (Nos. 20073014, 20103003), Doctor Foundation of Educational Ministry, Excellent Young Teacher Foundation of Ministry of Education of China and Excellent Young Foundation of Jilin Province. The authors are thankful for the reviewers' invaluable comments.

References

1. Kaiser RI (2002) Chem Rev 102:1309
2. Winnewisser G, Kramer C (1999) Space Sci Rev 90:181
3. Largo A, Barrientos C, Lopez X, Ugalde JM (1994) J Phys Chem 98:3985
4. del Rio E, Barrientos C, Largo A (1996) J Phys Chem 100:585
5. Zhan CG, Iwata S (1997) J Chem Phys 107:7323
6. Pascoli G, Lavendy H (1999) J Phys Chem A 103:3518
7. Li GL, Tang ZC (2003) J Phys Chem A 107:5317
8. Millar TJ (1991) Astron Astrophys 242:241
9. Sumiyoshi Y, Takada H, Endo Y (2004) Chem Phys Lett 387:116
10. McCarthy MC, Cooksy AL, Mohamed S, Gordon VD, Thaddeus P (2003) Astrophys J Suppl Ser 144:287
11. Yu GT, Ding YH, Huang XR, Chen GH, Tang AC (2004) J Phys Chem A 108:10723
12. Nakajima M, Yoneda Y, Sumiyoshi Y, Endo Y (2004) J Chem Phys 120:2662
13. Pedersen CT, Fanghanel E, Flammang R (2001) J Chem Soc Perkin Trans 2:356
14. Frisch MJ, Trucks GW, Schlegel HB, Scuseria GE, Robb MA, Cheeseman JR, Zakrzewski VG, Montgomery JA Jr, Stratmann RE, Burant JC, Dapprich S, Millam JM, Daniels AD, Kudin KN, Strain MC, Farkas O, Tomasi J, Barone V, Cossi M, Cammi R, Mennucci B, Pomelli C, Adamo C, Clifford S, Ochterski J, Petersson GA, Ayala PY, Cui Q, Morokuma K, Malick DK, Rabuck AD, Raghavachari K, Foresman JB, Cioslowski J, Ortiz JV, Stefanov BB, Liu G, Liashenko A, Piskorz P, Komaromi I, Gomperts R, Martin RL, Fox DJ, Keith T, Al-Laham MA, Peng CY, Nanayakkara A, Gonzalez C, Challacombe M, Gill PMW, Johnson BG, Chen W, Wong MW, Andres JL, Head-Gordon M, Replogle ES, Pople JA (1998) Gaussian 98, revision A.9. Gaussian, Inc., Pittsburgh
15. Karlström G, Lindh R, Malmqvist P-Å, Roos BO, Ryde U, Veryazov V, Widmark P-O, Cossi M, Schimmelpfennig B, Neogrady P, Seijo L (2003) Comput Mater Sci 28:222
16. Reed AE, Weinstock RB, Weinhold F (1985) J Chem Phys 83:735
17. Yu GT, Ding YH, Huang XR, Sun CC (2005) J Phys Chem A 109:1594
18. Ding YH, Liu JL, Huang XR, Li ZS, Sun CC (2001) J Chem Phys 114:5170